SMALL-SCALE FLARES AS THE CAUSE OF QUIET SUN EUV EMISSION

A. Pauluhn[1,2] **and S.K. Solanki**[2]

[1]*International Space Science Institute, CH-3012 Bern, Switzerland, email: pauluhn@issi.unibe.ch*
[2]*Max-Planck-Institut für Sonnensystemforschung, D-37191 Katlenburg-Lindau, Germany, email: solanki@linmpi.mpg.de*

ABSTRACT

In previous studies we have shown that the asymmetric radiance distributions of quiet Sun time series can be represented by lognormal distributions and modelled by small-scale flaring processes. We employ a stochastic model to describe the ensemble of small-scale flaring processes. Using this model, we confirm that the shape of the resulting radiance distributions is mainly dependent on the ratio between damping and excitation. We present parameter studies for flare energy distributions of various steepnesses. The synthetic time series are compared with SUMER data of long time series of transition region and coronal quiet Sun data.

1. INTRODUCTION

Solar transient events such as flares and micro- or nanoflares, explosive events and blinkers, have been the subject of a large number of studies, e.g., by Datlowe et al. (1974); Lin et al. (1984); Harrison (1997); Krucker & Benz (1998); Parnell & Jupp (2000); Brković et al. (2001); Aschwanden & Parnell (2002); Winebarger et al. (2002); Harrison et al. (2003). Many such transient brightenings are thought to have a common cause, namely magnetic reconnection. Via dissipation of the energy stored in the magnetic fields they provide a strong mechanism for heating the solar chromosphere and corona (Parker 1988).
The frequency distribution of the energy of flares, blinkers and explosive events (dN/dE) has been found to obey a power-law for several wavelength regimes. The observed exponents α in the power-law relation $dN/dE = E_0 E^{-\alpha}$ range from 1.5 to 2.9 for solar as well as for stellar flares. The width of this range is due mainly to uncertainties in determining this exponent. Exponents within this range are also obtained for blinkers and explosive events. The larger the exponent, the more weight is given to small-scale events such as micro- and nanoflares. For an exponent greater than 2, the energy content is dominated by the small-scale events and in order to have finite total energy content, a lower cutoff in energy has to be introduced. Events in the energy range $10^{30} - 10^{33}$ erg ($10^{23} - 10^{26}$ J) are usually referred to as "normal" flares. Nanoflares (Parker 1988) are the brightenings with energy below approximately 10^{27} erg, although the limits vary somewhat in the literature.
The radiation of the quiet Sun is often viewed as generated by a superposition of a large number of flares (Phillips and Dwivedi 2003). Thus, flare heating is a powerful concept for the heating of the outer parts of the solar and stellar atmospheres.

In this work we continue the studies introduced in Pauluhn and Solanki (2004), where it was shown that the time series of SUMER transition region measurements could well be represented with a simple model driven by a flaring process consisting of a stochastic part and a damping. We extend that work to higher temperature regimes using high-resolution SUMER data and confirm that the described stochastic flaring process is a suitable model for the quiet Sun EUV emission, also at temperatures representative of the low corona. The dependence of the simulated radiance distributions on the free parameters of the model is investigated, such as the exponent of the underlying flare amplitude distribution.
We begin with an outline of the model used for the flare simulation and repeat the theoretical reasoning for the radiances being lognormally distributed under the assumption that they are entirely due to transient events (Sect. 2). The results of parameter studies with our model are presented in Sect. 3. In Section 4 we present the results for the different temperature regions, and the conclusions are given in Sect. 5.

2. THE MODEL AND SIMULATION

The model to generate synthetic time series of EUV radiances has been described in Pauluhn and Solanki (2004). We presume that flaring is an intrinsically stochastic process, and our radiance variable is a time-dependent random variable, i.e., a stochastic process. One simulation thus delivers a possible realization of this process.
The radiance model simply consists of a time series of random kicks (acting as "flares"), applied to an initial value. Each kick is followed by the exponential decay of the radiance. The final radiance is given by the sum

of the radiances of all the overlapping transient brightenings.
Depending on the choice of the temporal profile of a single brightening event we have either 5 or 6 free parameters: the flare amplitude range and the power-law exponent, the e-folding or damping time of the flare, if we assume a single kick with a sharp rise and a successive exponential decrease. Additionally, in order to smooth the steep increase a rise time can be introduced. Furthermore, the frequency of the excitation, i.e., the flaring rate or flaring probability p_f, has to be determined.

The simulation involves the following steps:

1. Generate a distribution of flare magnitudes, i.e. (positive) values of flare amplitudes f_n.
2. Start from an initial radiance value $r_0 > 0$ (this can be the "first kick" from the flare distribution, $r_0 = f_0$).
3. At random time t_i another radiance r_i is generated by adding a flare kick f_i,
$$r_i = r_{i-1} + f_i. \quad (1)$$
4. At successive time steps t_j, $j > i$, the radiance values are
$$r_j = r_i \cdot \exp(-\frac{t_j - t_i}{\tau_d}), \quad (2)$$
multiplicatively generated from the preceding values, with τ_d the damping time.

The probability of a transient brightening occurring per time unit, p_f with $0 < p_f < 1$, is simulated by drawing equally distributed random numbers between 0 and 1, and a flare event is started at t_i if the random number falls within a certain fraction of the interval (0,1), e.g., a flaring probability of 30 % or 0.3 is realized by applying the kick if the random number is smaller than 0.3. The flare process is thus a Poisson process, which is equivalent to the fact that the waiting times, i.e., the time intervals between two flares ΔT_i, are exponentially distributed with parameter p_f, and the mean waiting time $< \Delta T >$ is given by $1/p_f$. Additionally to the excitation, we include a damping process of strength $k = \frac{1}{\tau_d}$. In Fig. 1 an example sequence of flares with very large mean waiting times or low frequency p_f is shown.

A heuristic explanation for the distribution of the radiances is given in the following. We assume that we can express the kick as $f_i = c \cdot r_{i-1}$, with c a positive value, i.e., the new radiance can be seen as
$$r_i = r_{i-1} + c \cdot r_{i-1} = \hat{c} \cdot r_{i-1}, \quad (3)$$
a multiple of the predecessor radiance. (We stress, however, that we prescribe the distribution of the additive components f_i, given, e.g., by observation as a power law, and not that of the multiplicative component c.)

Thus, the radiance value at the nth step is
$$r_n = r_0 \cdot c_1 \cdot c_2 \cdot \cdots \cdot c_n, \quad (4)$$

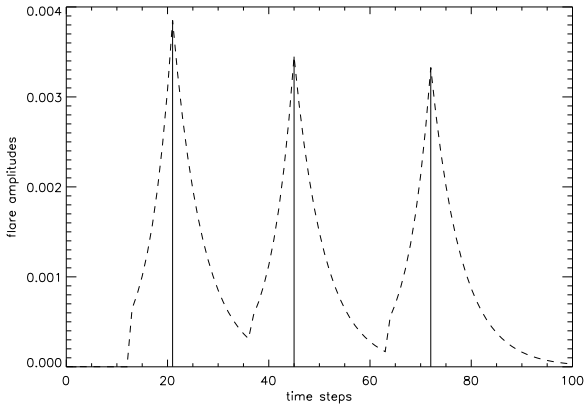

Figure 1. An example sequence of simulated flares. Here, the flaring frequency has been chosen to be very small, $p_f = 0.04$, such that the average waiting time between two flares is 25 time steps. For higher frequencies, the radiance is given as a superposition of the input kicks.

with the c_i being random factors if a new kick happens at this time. Otherwise c_i represents the damping or decay as described by the exponential in Eq. (2).

Taking the logarithm of this equation yields
$$\log(r_n) = \log(r_0) + \log(c_1) + \log(c_2) + \cdots + \log(c_n). \quad (5)$$

The Central Limit Theorem (applied to the logarithms), then states that as n goes to infinity, the distribution of the sum converges to a normal distribution. Thus, the distribution of the sum in Eq. (5) is normal, so that the distribution of the r_n is lognormal. The next step is the determination of the parameters of the lognormal distribution
$$\rho(x) = \frac{N_0}{\sigma x \sqrt{2\pi}} \exp(-\frac{(\log(x) - \mu)^2}{2\sigma^2}) \quad (6)$$
with $\mu =< \log(x) >$, $\sigma = \sqrt{Var(\log(x))}$ and N_0 a normalization factor.

This assumption of a multiplicative process is plausible in the light of the radiance being ultimately generated by emerging and decaying magnetic field. In Pauluhn and Solanki (2004) a (multiplicative) stochastic differential equation (i.e., a differential equation containing a stochastic or "noise" part) for the radiance and corresponding Fokker-Planck equation for its probability density function ρ (see, e.g., Risken 1989; Gardiner 1990; Honerkamp 1990) were derived for such a process. Under the described assumptions a stationary solution with a lognormal shape was found.

The two characterizing parameters of the stationary solution μ and σ have been determined empirically by parameter scans (Pauluhn and Solanki 2004), and the shape parameter σ has been found to be dependent on the ratio between damping (given by the damping parameter

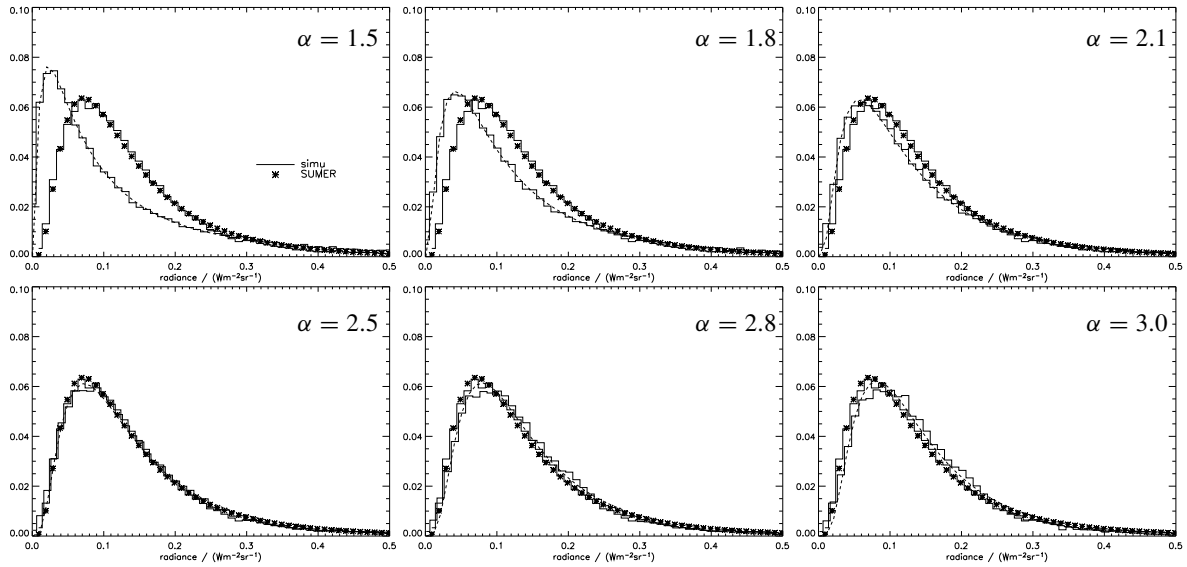

Figure 2. Variation of the radiance distribution (to be precise, the radiance probability density function) with the exponent α of the flare distribution. The following parameters have been kept constant: $p_f = 0.43$, $\tau_d + \tau_r = 5.72$ time steps, and $y_{max} = 0.8$. Also shown are a SUMER O IV network histogram and the corresponding lognormal fit.

$k = \frac{1}{\tau_d}$) and the stochastic excitation. The stochastic part of the process is given by the parameters of the Poisson flaring process, which is mainly the frequency p_f, and also the mean value of the input flare distribution which is dependent on the upper and lower amplitude boundaries and the exponent of the power law.

$$\sigma \sim \frac{1}{\sqrt{\tau_d p_f}}. \qquad (7)$$

3. COMPARISON WITH SUMER DATA AND PARAMETER STUDIES

SUMER data of the EUV lines O IV and Ne VIII were used for comparison. These lines represent temperatures of the transition region (O IV) and also of regions with higher temperatures, reaching into the lower coronal regime (Ne VIII). The model parameters were varied and matched to fit the SUMER measurements.

3.1. The SUMER data

On 8 February 1998, the SUMER instrument (Wilhelm et al. 1995) performed a long-duration observation of quiet areas near disk centre in the O IV and Ne VIII lines. SUMER is a stigmatic normal incidence telescope and spectrometer, operating in the wavelength range from 46.5 to 161.0 nm, depending on the spectral order and the choice of detector. The O IV line at 79.0 nm, and the Ne VIII line at 77.0 nm, which are used here, are measured in first order. The measurements, which have also been described by Wilhelm and Kalkofen (2003), were taken over 7 h and 20 min with a cadence of 33.5 s and an excellent pointing stability. The data were corrected for the flatfield, the geometric distortion, and for detector electronics effects such as dead-time and local-gain depression. After the instrumental corrections and the radiometric calibration, the solar radiances were determined by integration over the line profiles, which were derived by least-squares fits of single Gaussian functions and a linear background. The background (continuum) was subtracted prior to integration.

3.2. Dependence on the power law exponent

For constant flaring frequency and damping (and rise) time, the energy input to the system is determined by the flare distribution, i.e., the minimum and maximum flare amplitude and the exponent of the power law. In order to investigate the shape of the radiance distribution in dependence on the flare input distribution, we varied the exponent α. For fixed upper and lower boundaries, the energy input decreases with increasing exponent. Thus, in order to reproduce a certain (measured) radiance time series and its mean value, the (lower) boundary y_{min} has to be varied simultaneously with the exponent such as to keep the mean energy input constant.

$$< E >= \int_{y_{min}}^{y_{max}} E E^{-\alpha} \mathrm{d}E = \int_{y_{min}}^{y_{max}} E^{1-\alpha} \mathrm{d}E. \qquad (8)$$

We chose as "reference" the SUMER time series of the transition region 79.0 nm network area. Fig. 2 shows the resulting probability densities and cumulative distribution functions of the simulated time series and the

given SUMER data. The histograms have been computed over the ensemble of all network time series in the observed quiet-Sun area (60 pixels). For constant flare frequency $p_f = 0.43$, damping time $\tau_d + \tau_r = 5.72$ time steps (191.7 s) and constant upper amplitude value of $y_{max} = 0.8$, the value of α has been varied (α =1.5, 1.8, 2.1, 2.5, 2.8, 3.0), thereby also varying the y_{min} value (y_{min} =0.002, 0.006, 0.011, 0.016, 0.019, 0.021), such as to keep the energy input constant (as well as the number of flares). The results for the lognormal parameters μ and σ are shown in Fig. 3. The μ and σ of the lognormal fitted to the SUMER data were $\mu_S = -2.16$ and $\sigma_S = 0.98$, and the exponent $\alpha = 2.5$ yielded the best match, which was determined from a comparison of the density functions fitted to the histograms and the corresponding cumulative distribution functions.

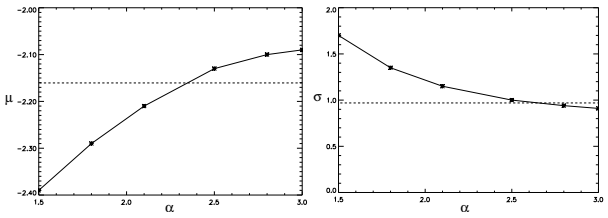

Figure 3. Variation of the lognormal parameters with the exponent α of the flaring input distribution. The mean total input has been held constant by varying the lower boundary of the flare amplitudes accordingly. The dashed lines show the corresponding lognormal-fit values to the SUMER data.

3.3. Dependence on the ratio of damping to noise

The equilibrium distribution is generally determined by the ratio of damping to excitation. Only when the two forces balance each other, can a stationary state be reached. To confirm this for our simulations, we vary the quotient $\frac{k}{p_f} = \frac{1}{\tau_d p_f}$ in two different ways: first, we vary τ_d and allow p_f to remain constant, and second, vice versa. The results are shown in Fig. 4. Within the uncertainties of the fits, both curves agree very well.

Where the damping or excitation exceed certain limiting values, no stable solution exists. If the excitation is too strong ($\frac{k}{p_f} \leq 0.1$), the realizations grow unboundedly, and on the other end of the range, if the ratio of $\frac{k}{p_f} = \frac{1}{\tau_d p_f}$ exceeds 1.2, the shape of the lognormal changes from a two-sided function to a function with a maximum value near zero and a rightwards extending tail.

The parameters τ_d and p_f were also both varied accordingly, such that the quotient remained constant. This left the parameters μ and σ of the simulated distribution constant, too.

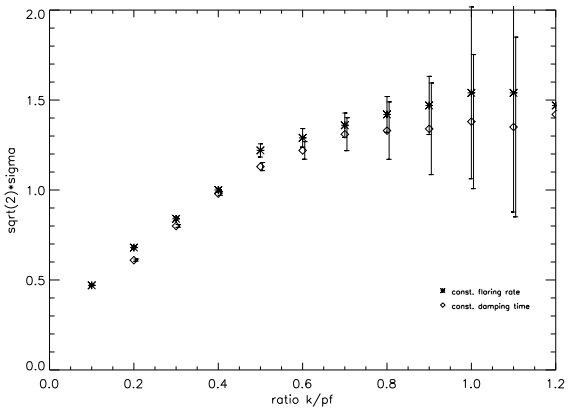

Figure 4. Variation of the lognormal shape parameter with the ratio of damping to flaring rate. The stars give the results for constant flaring rate p_f and varying damping time ($\tau_d + \tau_r$), and the squares give the results for constant damping time and varying flaring rate.

4. THE DISTRIBUTIONS FOR DIFFERENT TEMPERATURE REGIMES

In the simulations, the rise time was in all cases chosen to be 75 % of the damping time. Adding Poisson photon noise to the model realizations gives slightly better matches when comparing the single time series (see Figs. 5 to 8) and their histograms, but does not significantly improve the fits for the total cell or network areas (compare Fig. 2).

4.1. Transition region cells

The SUMER time series of the transition region line O IV could be well reproduced. The photon noise ($\sqrt{counts}$) was on average 7 % of the signal for the O IV data. The model parameters $p_f = 0.43$, $\tau_d + \tau_r = 5.72$ time steps (191.7 s), $\alpha = 2.5$, $y_{min} = 0.004$ and $y_{max} = 0.8$ turned out to be appropriate for the representation of the transition region cells (see Fig. 5).

4.2. Transition region network

The same parameters as for the cell regions were used, however, the amplitude of the input process had to be adjusted to be $y_{min} = 0.016$, in order to increase the energy of the smallest flares. The SUMER time series and a simulation are shown in Fig. 6.

4.3. Coronal cells

For higher temperatures, the time series exhibit different types of variability. The shapes of the probability density functions are narrower than for the transition region (Pauluhn et al. 2000). The superposition of at

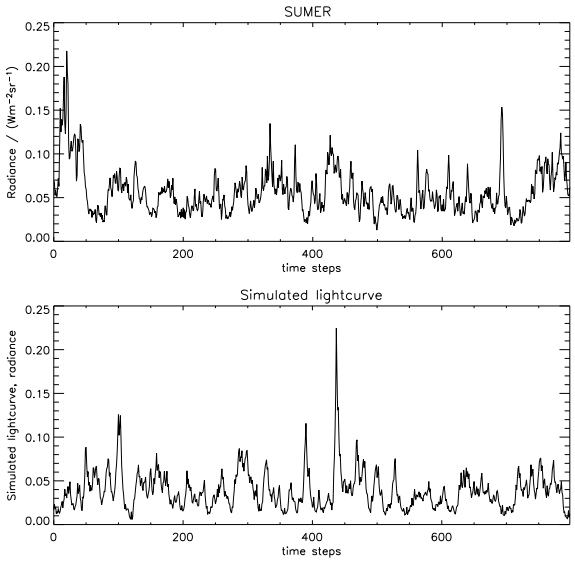

Figure 5. SUMER time series of a cell region (1 pixel) in the transition region line 79.0 nm, and a corresponding simulation with parameters $p_f = 0.43$*,* $\tau_d + \tau_r = 5.72$ *time steps,* $\alpha = 2.5$*,* $y_{min} = 0.004$*,* $y_{max} = 0.8$*.*

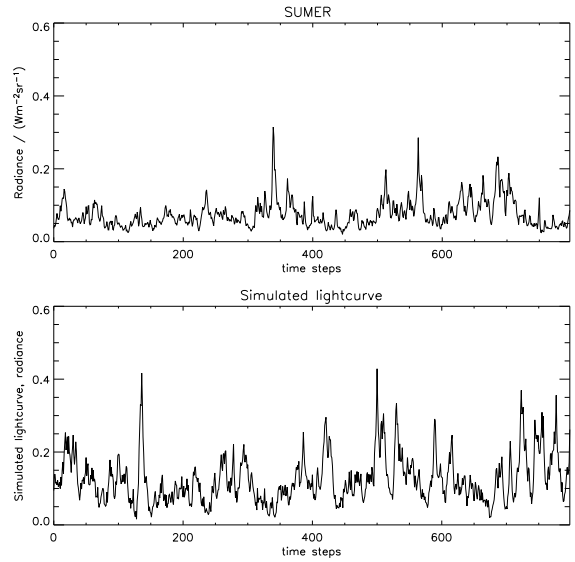

Figure 6. SUMER time series of a network region (1 pixel) in the transition region line 79.0 nm, and a corresponding simulation with parameters $p_f = 0.43$*,* $\tau_d + \tau_r = 5.72$ *time steps,* $\alpha = 2.5$*. Only the lower amplitude boundary for the flare process has been chosen differently relative to the cell interior:* $y_{min} = 0.016$*.*

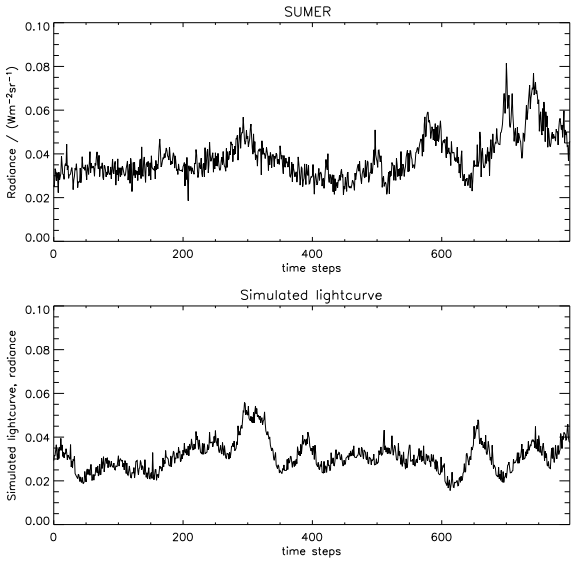

Figure 7. SUMER time series of a cell region (1 pixel) in the upper transition region/coronal line 77.0 nm, and a corresponding simulation with parameters $p_f = 0.11$*,* $\tau_d + \tau_r = 44.40$ *time steps (1487.5 s),* $\alpha = 2.5$*,* $y_{min} = 0.003$*,* $y_{max} = 0.02$*.*

least two process scales, one low-frequent and weakly damped for the background, another stronger damped and higher variable are clearly recognizable. The time series of the single cells could be well represented by a weakly damped and low-frequent flare excitation, such as $p_f = 0.11$, $\tau_d + \tau_r = 44.40$ time steps (1487.5 s), $\alpha = 2.5$, $y_{min} = 0.003$, $y_{max} = 0.02$, and a superposed roughly 9 % photon noise process (see Fig. 7).

4.4. Coronal network

Although a simulation with the parameters $p_f = 0.45$, $\tau_d + \tau_r = 26.64$ time steps (892.5 s), $\alpha = 2.5$, $y_{min} = 0.003$, $y_{max} = 0.0045$ delivered satisfactory results, a slight dependence of the damping time on the amplitude was tested, and was found to improve the correspondence between the data and the simulation results. Higher amplitudes were assumed to be stronger damped, and lower ones to be more weakly damped, in order to provide part of the background radiance. The dependence was given as a linear relation:

$$\tau_d = \frac{1}{2}\tau_{d0}\left(\frac{y_{max} - y}{y_{max} - y_{min}} + 1\right), \qquad (9)$$

such that the maximum damping time τ_{d0} is employed for the smallest flares around y_{min} and the minimum damping time $\frac{1}{2}\tau_{d0}$ is used for the flares with amplitudes around y_{max}. Using the amplitude-dependent damping, the model parameters were $p_f = 0.57$, maximum $\tau_d + \tau_r = 22$ time steps (735 s), $\alpha = 2.5$, $y_{min} = 0.003$, $y_{max} = 0.0045$ (see Fig. 8). High-frequency low-amplitude flaring dominates the network at higher temperatures.

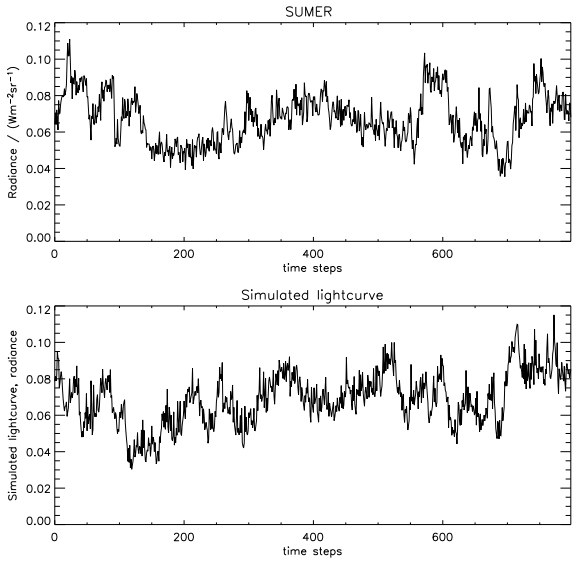

Figure 8. SUMER time series of a network region (1 pixel) in the upper transition region/coronal line 77.0 nm, and a corresponding simulation with parameters $p_f = 0.57$*, maximum* $\tau_d + \tau_r = 22$ *time steps (735 s),* $\alpha = 2.5$*,* $y_{min} = 0.003$*,* $y_{max} = 0.0045$*. In this example, the lightcurve has been simulated with slightly amplitude-dependent damping time (see text for details).*

4.5. Discussion

The simulations show that multiplicative stochastic processes are suitable models for solar transient brightenings also for higher temperatures than those of the transition region. The shape and scale of the resulting lognormal histograms of the radiances are strongly dependent on the ratio of the damping to the excitation process. Best simulation results were achieved for power law exponents of around 2.5. We estimate an uncertainty from the fitting procedure as ± 0.2. Note that this value is obtained assuming that all (nano-)flares cover the same geometrical size. The dissipation time scales of the corona are found to be significant larger than in the transition region (by a factor of 4 to 8), which is consistent with theory. In order to cover "background flaring" as well as flaring with higher amplitude, a superposition of two or more processes with different time scales and amplitudes is needed. This is especially the case for the higher temperature time series. We have modelled part of this by including an amplitude-dependent damping in part of the simulations.

5. SUMMARY AND CONCLUSIONS

We have shown that a simple model of randomly generating a time series of radiances by (flare-)excitation can approximately reproduce measured quiet Sun statistics of transition region as well as of coronal lines. It was confirmed that the stationary radiance distribution is dependent on the ratio of the excitation and the damping processes. We have also studied the dependence on the exponent α of the power-law input distribution. Further studies are required to investigate more thoroughly the possible amplitude dependence of the damping within the flaring mechanism.

ACKNOWLEDGEMENTS

SOHO is a project of international cooperation between ESA and NASA.

REFERENCES

Aschwanden, M.J., & Parnell, C.E. 2002, *Astrophys. J.*, 572, 1048

Brković, A., Solanki, S. K., & Rüedi, I. 2001, *A&A*, 373, 1056

Datlowe, D.W., Elcan, M.J., & Hudson, H.S. 1974, *Sol. Phys.*, 39, 155

Gardiner, C.W. 1990, *Handbook of Stochastic Methods*, 2nd edition, Springer-Verlag, New York, Berlin, Heidelberg

Harrison, R. A. 1997, *Sol. Phys.*, 175, 467

Harrison, R. A., Harra, L. K., Brković, A., & Parnell, C. E. 2003, *A&A*, 409, 755

Honerkamp, J. 1990, *Stochastische Dynamische Systeme*, VCH, Weinheim, Germany

Krucker, S., & Benz, A.O. 1998, *Astrophys. J.*, 501, L213

Lin, R.P., Schwartz, R.A., Kane, S.R., Pelling, R.M., & Hurley, K.C. 1984, *Astrophys. J.*, 283, 421

Parker, E.N. 1988, *Astrophys. J.*, 330, 474

Parnell, C.E., & Jupp, P.E. 2000, *Astrophys. J.*, 529, 554

Pauluhn, A., Solanki, S.K., Rüedi, I., Landi, E., & Schühle, U. 2000, *A&A*, 362, 737

Pauluhn, A., & Solanki, S. K. 2004, *ESA SP-547*, 323

Phillips, K. J. H., & Dwivedi, B. N. 2003, *Dynamic Sun*, Cambridge University Press, 335

Risken, H. 1989, *The Fokker-Planck Equation*, 2nd edition, Springer-Verlag, New York, Berlin, Heidelberg

Winebarger, A. R., Emslie, A. G., Mariska, J. T., & Warren, H. P. 2002, *Astrophys. J.*, 565, 1298

Wilhelm, K., Curdt, W., Marsch, E., et al. 1995, *Sol. Phys.*, 162, 189

Wilhelm, K., & Kalkofen, W. 2003, *A&A*, 408, 1137